A Novel Technique for Nowcasting Extreme Rainfall Events using Early Microphysical Signatures of Cloud Development

SINAN NIZAR[1], Jobin Thomas[2], P J Jainet[3], and K P Sudheer[2]

[1]Institute For Climate Change Studies
[2]Indian Institute of Technology Madras
[3]Centre for Water Resources Development and Management

November 26, 2022

Abstract

The extensive damages of extreme rainfall events (EREs) and associated natural disasters on the natural and anthropogenic resources and the enormous economic losses underscore the requirement for developing early warning systems to mitigate the impact of such disasters. However, accurate forecasting of EREs at a regional scale and at higher lead times is challenging due to the uncertainties involved in the model predictions. This study proposes a novel technique to nowcast the heavy and extreme rainfall events using the early signatures of the microphysical evolution of mesoscale convective clouds. The nowcasting method integrates the cloud top temperature (T)-cloud effective radius (re) profile derived using remote sensing methods and logistic regression modelling to estimate the probability for the occurrence of heavy and extreme rainfall events. The capability of the method is demonstrated by nowcasting different recent EREs over the windward slopes of the southern Western Ghats (Kerala, India). The results of the analysis of the T-re profiles of the normal, heavy and extreme rainfall events of August 2018 are significantly distinct and indicates polluted (aerosol-rich) scenario during EREs. The study suggests significant interactions between moisture availability and aerosol concentration during the occurrence of EREs in August 2018, along with their independent effects. The proposed technique shows distinctive competency for nowcasting the EREs at a regional scale with an overall accuracy of 93% and at a lead time of not less than six hours. This study highlights the significance of the aerosol-cloud interactions in the occurrence of EREs of the region and suggests the importance of the aerosol pollution leading to EREs and associated natural disasters.

Posted on 26 Nov 2022 — CC-BY-NC-ND 4 — https://doi.org/10.1002/essoar.10511599.1 — This a preprint and has not been peer reviewed. Data may be preliminary.

A Novel Technique for Nowcasting Extreme Rainfall Events using Early Microphysical Signatures of Cloud Development

Sinan Nizar[1], Jobin Thomas[2], P. J. Jainet[3,4], and K. P. Sudheer[*1,2,5,6]

[1]Institute for Climate Change Studies, Kottayam 686 104, India. [2]Department of Civil Engineering, Indian Institute of Technology Madras, Chennai 600 036, India. [3] KSCSTE – Centre for Water Resources Development and Management, Calicut, India. [4]Department of Civil Engineering, Indian Institute of Technology Palakkad, Palakkad 678557, India. [5]Department of Agricultural and Biological Engineering, Purdue University, West Lafayette, IN, USA. [6]Kerala State Council for Science Technology and Environment, Thiruvananthapuram 695 004, India.

*Corresponding author - e-mail: sudheer@iitm.ac.in

Abstract

The extensive damages of extreme rainfall events (EREs) and associated natural disasters on the natural and anthropogenic resources and the enormous economic losses underscore the requirement for developing early warning systems to mitigate the impact of such disasters. However, accurate forecasting of EREs at a regional scale and at higher lead times is challenging due to the uncertainties involved in the model predictions. This study proposes a novel technique to nowcast the heavy and extreme rainfall events using the early signatures of the microphysical evolution of mesoscale convective clouds. The nowcasting method integrates the cloud top temperature (T) - cloud effective radius (r_e) profile derived using remote sensing methods and logistic regression modelling to estimate the probability for the occurrence of heavy and extreme rainfall events. The capability of the method is demonstrated by nowcasting different recent EREs over the windward slopes of the southern Western Ghats (Kerala, India). The results of the analysis of the T-r_e profiles of the normal, heavy and extreme rainfall events of August 2018 are significantly distinct and indicates polluted (aerosol-rich) scenario during EREs. The study suggests significant interactions between moisture availability and aerosol concentration during the occurrence of EREs in August 2018, along with their independent effects. The proposed technique shows distinctive competency for nowcasting the EREs at a regional scale with an overall accuracy of 93% and at a lead time of not less than six hours. This study highlights the significance of the aerosol-cloud interactions in the occurrence of EREs of the region and suggests the importance of the aerosol pollution leading to EREs and associated natural disasters.

Keywords: Nowcasting; aerosols; cloud-microphysics; extreme rainfall events

1. Introduction

Extreme rainfall events (EREs), leading to flash floods and landslides, pose a significant risk to life, agriculture, infrastructure, and livelihood.The frequency of occurrence of EREs is expected to increase in the warming climate with increased atmospheric moisture transport (Hamada et al., 2015; Kumar et al., 2019). Mitigation of the impacts of EREs and the consequent natural disasters needs focused attention to reduce the economic and societal losses. However, accurate forecasting of EREs at a regional scale and at higher lead times is still challenging despite the recent scientific advances in numerical weather prediction capabilities, as the predictions are embedded with uncertainties generated from different sources (Mao et al., 2018; Srinivas et al., 2018; Wang et al., 2021). On the other hand, significant improvements have been achieved in the nowcasting of EREs using remote sensing-based observations of active meteorological systems

(Fortelli et al., 2019). Numerical weather prediction (Wilson et al., 1998; Radhakrishna et at., 2012; Sun et al., 2014), radar extrapolation (Li and Lai, 2004; Fox and Wikle, He et al., 2013; Xiang et al., 2020; Ravuri et al., 2021) and stochastic models (Sirangelo et al., 2007; Metta et al., 2009; Pulkkinen et al., 2019) are the standard methods of nowcasting EREs. However, these methods rely on large corpora of high-resolution observation networks such as Doppler weather radars, automatic weather stations, wind profilers, and radiometers that monitor and deliver reliable data at short spatial and temporal intervals. In regions with scarce ground observations, remote sensing-based observations of active meteorological systems, have demonstrated their great potential for nowcasting EREs.

The nowcasting of EREs using remote sensing data usually relies on cloud top temperature (T) as a key signature of cloud development (e.g., Shukla et al., 2017). However, the occurrence of EREs is strongly influenced by numerous additional factors related to the internal dynamics and microphysics of mesoscale convective systems (Ahmed and Schumacher, 2015; Roca and Fiolleau, 2020). For instance, aerosol pollution/enrichment influences the cloud development and precipitation formation processes (Guo et al., 2015; Zhao et al., 2010), and the increasing concentration of anthropogenic aerosols modify the cloud microphysical processes (Rosenfeld et al., 2008). The knowledge about the cloud microphysical processes and cloud-aerosol interactions is presumably critical in the accurate forecasting/nowcasting of the EREs (Mao et al., 2018). The existing remote sensing-based methods of nowcasting do not consider aerosol-cloud interactions and the consequent changes in the cloud microphysical evolution, which is a major limitation for accurate nowcasting of EREs. Rosenfeld and Lensky (1998) suggested that the vertical evolution of cloud effective radius (r_e) is an indicator of the cloud development leading to the occurrence of EREs. The present study proposes a method that uses the satellite-derived T-r_e profile to nowcast EREs at a regional scale, and is demonstrated using the data pertaining to the recent EREs in Kerala, highlighting the significance of the aerosol-cloud interactions in the EREs of the region and suggest the importance of the aerosol enrichment (pollution). The windward slopes of the Western Ghats (eg., Kerala State of India) experienced unprecedented and widespread EREs consecutively in the last four years (2018 – 2021), which caused extensive flooding (in the lowlands) and numerous landslides (in the highlands) across the region (Fig. S1). Though the proposed nowcasting model is not specific to any geography, its performance evaluation in such a densly populated region experiencing strong monsoonal flow could reinforce its accuracy.

2. Material and Methods

The development of the nowcasting technique involves three major components: (1) general characterisation of the EREs, (2) assessment of T-r_e profiles of the different rainfall events in

August 2018, and (3) nowcasting of EREs using the variables derived from the T-r_e profiles and particle size distribution of clouds. The methodology is demonstrated using the information pertaining to the EREs experienced in Kerala State (between 2001-2018) with particular emphasis to the EREs occurred in August 2018. The details of the data used and the methodology adopted are given in the following sections.

2.1. Characterisation of EREs

The rainfall events of Kerala between 2001 and 2018 were extracted from the India Meteorological Department (IMD) gridded precipitation dataset at a spatial resolution of 0.25° x 0.25° (Pai et al., 2014). Following the guidelines of the IMD (Forecasting Circular No. 5/2015/3.7), the rainfall events over Kerala were regrouped, based on the accumulated daily rainfall depth value, into three: extreme, heavy and normal rainfall events. The rainfall events with a daily rainfall depth exceeding 204.4 mm were classified as EREs. The daily rainfall depth of less than 115.6 mm was considered a normal rainfall event, and the transitional range from 115.6 mm to 204.4 mm was classified as a heavy rainfall event.

The rainfall events of August 2018 were analysed using the total precipitable water vapour (TPWV) and aerosol loading over the region. Since the vertically integrated moisture flux provides prior information of the imminent heavy rainfall activity, the TPWV data were used to assess the moisture availability. The TPWV data for this study were extracted from the Modern-Era Retrospective analysis for Research and Applications, version 2 (MERRA-2; GMAO, 2015) reanalysis data, which are available at a spatial resolution of 0.5° x 0.5° and a temporal resolution of 1 hour. The significance of aerosol columnar content in the occurrence of EREs of the region was investigated by analysing the aerosol optical depth (AOD) data from the Moderate Resolution Imaging Spectroradiometer (MODIS) instrument. Numerous researchers have extensively validated the MODIS AOD products (Choudhry et al., 2012; Misra et al., 2015; Sayer et al., 2013; Tripathi et al., 2005). The daily AOD (550 nm) from Collection 6.1, level 3 AOD products (1°) derived from Terra's MODIS measurements, was used in this study. Further, the independent and interaction effects of the moisture availability and aerosol loading were assessed using the two-way analysis of variance (ANOVA) on the 18 years (2001-2018) of data of the Indian summer monsoon season.

2.2. Assessment of T-r_e profile of rainfall events

The evolution of cloud particles through various cloud microphysical stages leading to precipitation can be inferred from the characteristic T-r_e profile for convective systems (Rosenfeld and Lensky, 1998). The hourly cloud properties (of August 2018), such as T and r_e, were acquired from the NASA Langley Cloud and Radiation Research Group (http: //www-angler.larc.nasa.gov). The NASA-Langley cloud and radiation products are produced using the Visible Infrared Solar-infrared Split-Window Technique, Solar-infrared Infrared Split-Window Technique, and Solar-infrared Infrared Near-Infrared Technique (Minnis et al., 2008). Satellites retrieve r_e by measuring the statistical moment of cloud drop size distribution described by Nakajima and King (1990) and can be represented as Eq. 1.

$$r_e = \frac{\int_0^\infty r^3 n(r)dr}{\int_0^\infty r^2 n(r)dr} \tag{1}$$

where n(r) is the concentration of cloud radius having radius r. For a given temperature, r_e is assumed to be a conserved property (Rosenfeld and Lensky, 1998). Thus, the temporal evolution of individual cloud particles can be inferred from a single satellite image with multiple cloud particles at different stages of vertical development. In this study, the T-r_e relationship was assessed using the following steps (after Rosenfeld and Lensky (1998). First, the RGB image composed of red for visible reflectance, green for 3.9 μm brightness temperature, and blue for 10.8 μm brightness temperature were compiled to identify convective cloud clusters. With the aid of the RGB composite image, a window containing cloud elements representing all cloud growing stages were defined. Further, the 10, 25, 50, 75, and 90 percentiles of r_e for each 1°C interval of T was calculated. The percentiles indicate the sampling amount for each 1°C interval of T. The shape of the 50th percentile (median) was analysed to ascertain the various microphysical stages. The characteristics of the T-r_e curve, implying the different microphysical stages of cloud development used for the nowcasting procedure, were extracted from the median curve, as is illustrated in Fig. 1.

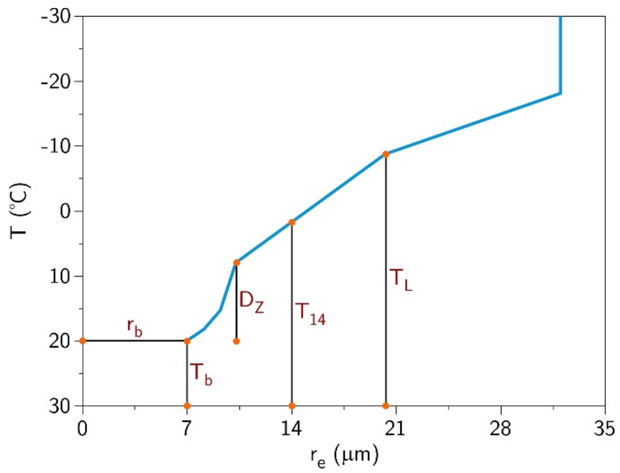

Fig. 1: Conceptual diagram illustrating various attributes extracted from the T-r_e curve. Cloud base temperature (T_b), the cloud base particle size (r_b), depth of the diffusional zone (D_z), cloud height in terms of temperature exceeding the 14 μm precipitation threshold (T_{14}), and the mixed-phase initiation height (T_L) were extracted from the T-re curve.

In convective clouds, droplets grow mostly by diffusion near the base such that r_e is proportional to D_a, where D_a is the depth above cloud base approximated by the cloud base temperature (T_b). Thus, T_b and the cloud base particle size (r_b) were extracted from the T-r_e curve. Since the polluted (aerosol-rich) environments have a more probable number of activated cloud condensation nuclei (CCN) at the cloud base, such cases are often marked by deep diffusional zones, which can be extracted as the depth of the diffusional zone (D_z). Coalescence and cloud formation processes amplify the particle growth rate and are crucial to the precipitation process. The coalescence growth of droplets becomes efficient beyond the r_e, crit of ≈ 14 μm. Therefore, the cloud height in terms of the temperature exceeding the 14 μm precipitation threshold (T_{14}) was extracted. Cloud droplets grow faster with height during the mixed-phase and can be identified as a sudden change in the slope of the T-r_e curve. As the contribution of mixed-phase processes is essential for an ERE, the mixed-phase initiation height is extracted from the T-r_e curve as T_L. The particle size distribution of clouds during normal, heavy and extreme rainfall events reveals distinct profiles. The heavy and extreme rainfall events are bimodal compared to normal rainfall events (Fig. 2). The first peak occurs at 14 μm (D_{14}) and the second at 70 μm (D_{70}), where the second peak is probably due to larger ice particles held by stronger updrafts during heavy/ extreme rainfall events. Thus, the ratio $\frac{D_{14}}{D_{70}}$ was also extracted.

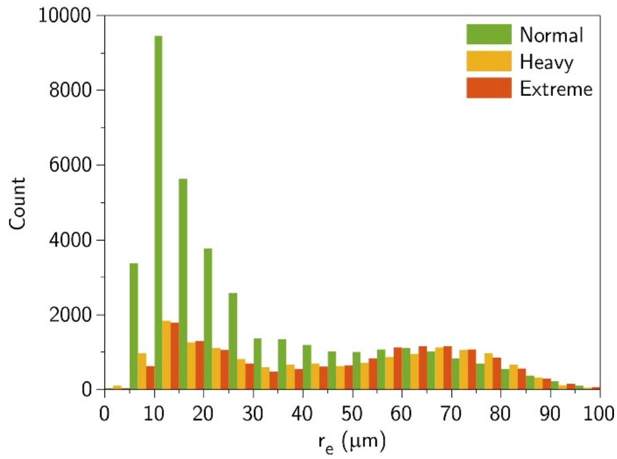

Fig. 2: Particle size distribution of cloud particles during normal, heavy, and extreme rainfall events. The particle size distribution of clouds during normal, heavy and extreme rainfall events reveals distinct profiles. The heavy and extreme rainfall events exhibit dual peaks compared to normal rainfall events: first peak around 14 μm (D_{14}) and the second one around 70 μm (D_{70}).

2.3. Nowcasting of EREs

The variables extracted from the T-r_e profile were used for the nowcasting of EREs. Logistic regression was fitted on the attributes extracted from the T-r_e curve to nowcast the EREs in terms of their probability of occurrence. The coefficients of the logistic regression for the variables were estimated using Eq. 2.

$$\frac{prob_{event}}{1-prob_{event}} = e^{-b_0-b_1r_b-b_2T_b-b_3D_Z-b_4T_{14}-b_5T_L} \qquad (2)$$

where b_0, b_1, b_2, b_3, b_4, and b_5 are the regression coefficients. The process of estimating the logistic coefficients is similar to that used in multiple regression except that, instread of using ordinary least squares as a mean of estimating the model, the maximum likelihood method is used. The model was fitted for the Monsoon month of August 2018 witnessing normal, heavy, and extreme rainfall events. Once the coefficients are estimated, the probability for the occurrence of heavy and extreme rainfall at any given time can be estimated using the variables extracted from the T-r_e curve at that time. The half-hourly gauge calibrated precipitation product from the Integrated Multi-Satellite Retrievals (IMERG; Huffman et al., 2019) was used to validate the accuracy of the nowcasting technique by comparing the probability of occurrence for EREs and the corresponding rainfall intensity at an hourly time scale.

3. Results and Discussion

3.1. Characterisation of the EREs over Kerala (2001-2018)

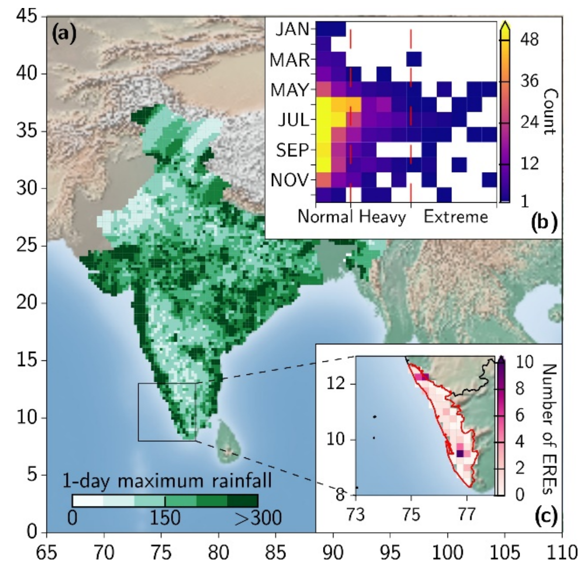

Fig. 3: Rainfall characteristics over the study area: (a) One-day maximum rainfall (2001 to 2018) based on the 0.25° x 0.25° gridded rainfall dataset (Pai et al., 2014) for the Indian sub-continent, **(b)** temporal distribution of normal, heavy and extreme rainfall events in terms of the frequencies of occurrence, and **(c)** frequency of EREs in the analysed domain (enclosed by the black rectangle) during the period. Only the rainfall values above 64.5 mm are plotted in **(b)**.

The analysis of the rainfall events over Kerala from 2001 to 2018 indicates that the region experienced 222 heavy rainfall events (daily rainfall depth > 115.6 mm) during the period, among which 32 were EREs (i.e., daily rainfall depth > 204.4 mm). Although the probability for the occurrence of EREs is very low (i.e., exceedance probability less than 1%) in the region, recent years (2018, 2019, and 2020) witnessed the occurrence of multiple EREs across Kerala due to large-scale moisture convergence below 800 hPa (Mukhopadhyay et al., 2021). The monthly rainfall of Kerala of August 2018 was 96% excess than normal, while the region received large excess (123%) rainfall during August 2019. The ERE of August 2018 recorded 319 mm of maximum daily rainfall, one of the most extreme events recorded in the last century. Among the 32 EREs in Kerala between 2001 and 2018, roughly 65% of the events occurred during the Indian summer monsoon season (mostly in July and August) (Fig. 3b). Although most regions of Kerala experienced EREs during the period, frequent occurrences are clustered around 9° 30’ N and 12° N latitudes (Fig. 3c). However, as a departure from this general pattern, Kerala witnessed widespread EREs in 2018 and 2019. Hence, the EREs of August 2018 were analysed in detail to understand the effect of moisture availability and aerosol loading on the occurrence of the EREs.

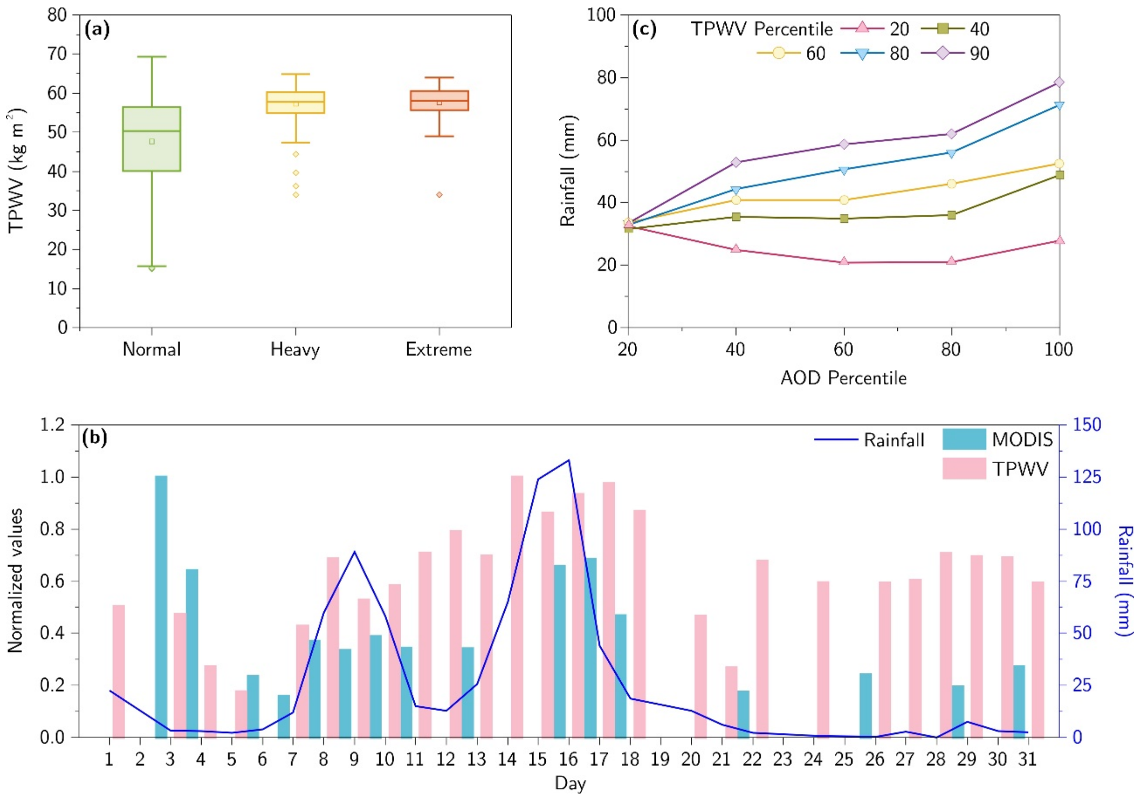

Fig. 4: Effect of moisture availability and aerosol loading on EREs: **(a)** variability of moisture availability (in terms of the TPWV) during normal, heavy, and extreme rainfall events between 2001 and 2018, **(b)** time series of daily TPWV, rainfall, and collection 6.1, level 3 Terra’s MODIS AOD during August 2018, and **(c)** mean rainfall profile for the different percentile classes of AOD and TPWV.

One of the major ingredients conducive for the occurrence of EREs is moisture advection, which is governed by various synoptic-scale features (Breugem et al., 2020). Temporal variability of the TPWV of the normal, heavy and extreme rainfall events (between 2001 and 2018) is shown in Fig. 4a. Despite the overlaps between the types of rainfall, the extreme and heavy rainfall events are characterised by relatively larger TPWV values than normal rainfall events. Obviously, a large moisture influx is necessary to form precipitating clouds that could yield heavy rainfall. Indeed, low-level jets and atmospheric rivers are the two major large-scale meteorological structures responsible for large-scale atmospheric moisture transport during heavy and extreme rainfall events in the region (Lyngwa and Nayak, 2021; Xavier et al., 2018). The intensification of the monsoon low-level jet core speed, westerly wind depth, zonal water vapour flux, horizontal wind shear and cyclonic vorticity brings a sufficiently large supply of moisture and triggers strong convection resulting in the occurrence of EREs during the Indian summer monsoon season (Xavier et al., 2018). The geographic setting of Kerala in the Indian peninsula along the western coast ensures sufficient moisture supply during the monsoon season with an increasing trend of near-surface water vapour over the tropical Indian Ocean (Rajeevan et al., 2008). The significance of the anomalously large amount of moisture supply from the neighbouring oceans in the EREs of August 2018 in Kerala was discussed by Lyngwa and Nayak (2021) and Mohandas et al. (2020), and the former observed that the air parcels had high moisture content near the Indian Ocean and increased in moisture over the Arabian Sea. However, all the events with higher TPWV values did not result in heavy or extreme rainfall events (Fig. 4a), which hints at the importance of other factors, such as concentration of CCN in the cloud formation processes produce heavy or extreme rainfall events.

The analysis of the wind trajectories of August 2018 indicates transport of aerosols from the Arabian Sea and the Indian Ocean, the Arabian Peninsula, and the Indo-Gangetic plains (Fig. S2), implying the significance of dust, mixed (dust-anthropogenic) aerosols, and sea-salt in the occurrence of EREs in the regional context. Atmospheric aerosols can alter the number and size of cloud drops, cloud lifetime, cloud microphysics and eventually, the precipitation formation (Kaufman et al., 2002; Ramanathan, 2001). In addition to the availability of atmospheric moisture, the formation of the cloud droplet from the available atmospheric moisture relies on the fraction of aerosol particles that serve as CCN. However, the interaction between moisture availability and aerosol concentration is non-linear and somewhat complex.

Temporal variability of the MODIS AOD, moisture availability, and rainfall during August 2018 is shown in Fig. 4b. A higher concentration of aerosols with a low moisture supply tends to form a large number of smaller cloud droplets, thus inhibiting processes leading to the occurrence of rainfall. Such conditions were noted on 3 and 4 August 2018. A similar suppressing effect as a result of increased CCN on precipitation to shut off warm rain process in convective tropical clouds was discussed by Rosenfeld (1999). Definitely, such cases result in low collision rates delaying raindrop formation (Khain et al., 2005). On the contrary, smaller AOD with sufficient moisture supply leads to the formation of a lesser number of large droplets. The ambient supersaturation, in those cases, is weakly consumed by the limited CCN resulting in faster growth of limited droplets that fall quickly as weak rain (Koren et al., 2014). The days 1, 7, 11, and 13 of August 2018 are examples of such scenarios leading to normal rainfall events. Indeed, the high rainfall events are characterised by significantly higher AOD along with sufficient moisture supply. An increase in rainfall is observed with an increase in the AOD at larger TPWV conditions (Fig. 4c), while for the lower TPWV conditions, an increase in the AOD shows low rainfall due to the formation of a larger number of smaller droplets. Similar observations of increased rainfall with aerosol concentrations in deep clouds having high liquid-water content were shown by Li et al. (2011). Over the Indian summer monsoon region, such scenarios of increased surface rainfall during polluted cases were shown by Choudhury et al. (2020) and Sarangi et al. (2017).

Table. 1: The independent and interaction effects of aerosols and moisture availability on rainfall over Kerala.

Source of variation	F	F_{cric}	$P-value$
AOD	17.22725	2.3813	1.19E-13
TPWV	36.68272	2.3813	1.53E-28
Interaction	2.826614	1.6541	0.000165

The results of the ANOVA show the significant role of the AOD and TPWV and their interaction on the occurrence of rainfall of the region ($p \leq 0.001$; Table 1). It may be noted that the aerosol concentration over Kerala shows a significant increasing trend (Fig. S3) which could invigorate cloud formation and intensify rain rates (Koren et al., 2012). The significant increase in aerosol loading over Kerala could impact the radiation budget (Ramanathan et al., 2005; Schwartz, 1996) and the cloud lifetime and their microphysics (Steinfeld, 1998; Twomey, 1977). Hence, it is expected to increase the occurrence of EREs over the region with the increasing atmospheric water holding capacity (IPCC, 2007) and the increasing trend of column integrated water vapour over the Indian Ocean (Trenberth et al., 2005) as a response to the climate warming.

3.2. Variation of the T-r_e profiles between normal, heavy and extreme rainfall events

The daily plots of the T-r_e profile were analysed to study the vertical evolution of cloud particles. Figure 5 shows three cases of cloud clusters resulting in normal (Fig. 5a), heavy (Fig. 5b) and extreme rainfall events (Fig. 5c) in August 2018. During EREs (Fig. 5f), the T-r_e profile is characterised with condensation dominated diffusional zone above the cloud base. The diffusional zone is initiated as the expansion of rising moist air increases the ambient supersaturation, and the excess vapour activates the aerosol particles by condensation, forming activated cloud droplets. The r_e is not sufficiently large enough (r_e < 14 μm) to support the warm rain process (Freud and Rosenfeld, 2012; Suzuki et al., 2010). The number of the activated cloud droplets (N_a) at the cloud base for a specific cloud base updraft velocity is determined by the number of CCN (N_{CCN}) (Rosenfeld, 2018). In highly polluted conditions, a large number of aerosol particles provides sufficient N_{CCN} for cloud formation. Each activated cloud droplet acts as a tiny sink adsorbing excess water vapour. Higher N_a produces more but smaller cloud droplets with a narrow size distribution resulting in a less efficient collision-coalescence process. The cloud droplets grow much slower during the diffusional zone reaching colder altitudes with smaller r_e, delaying collision-coalescence. As the depth of the diffusional zone is primarily determined by N_a (Rosenfeld et al., 2014), the deep diffusional zone during EREs (Fig. 5f) indicates higher N_a, which implies a polluted scenario. Though shallower, the heavy rainfall events are also marked with diffusional zones above the cloud base. However, the normal rainfall events are devoid of the diffusional zone and are characterised by the collision-coalescence region above the cloud base. Faster growth in r_e is observed until it stabilises around 14 μm. Moreover, this is a case of a clean environment with less N_{CCN} producing low N_a. The CAIPEEX study also showed similar cases of clouds with low N_a while developing in less polluted conditions of lower N_{CCN} (Konwar et al., 2012). The limited activated cloud droplets absorb most of the excess vapour and grow much faster in radius resulting in a smaller number of large cloud droplets with increased chances of collision and subsequent coalescence. The stabilisation of r_e at around 14 μm with further vertical growth during normal rainfall events is an indication of the warm rain process. Using a cloud parcel model, Rosenfeld (2002) showed that the rainwater fraction increases sharply for r_e above 14 μm. This is also evident from the simultaneous stabilisation of 75 percentile of r_e at a radius of 25 μm (Fig. 5d). The presence of cloud droplets with the r_e of 25 μm breaks the colloidal stability of the cloud, resulting in an efficient collision-coalescence process (Lamb, 2003). The warm rain mechanism thus established larger cloud droplets from the cloud tops, balancing additional coalescence, rendering the observed stabilisation of r_e (Rosenfeld, 2018). Such a warm rain process could also lead to rain washout of aerosols, thus limiting CCN for further cloud growth.

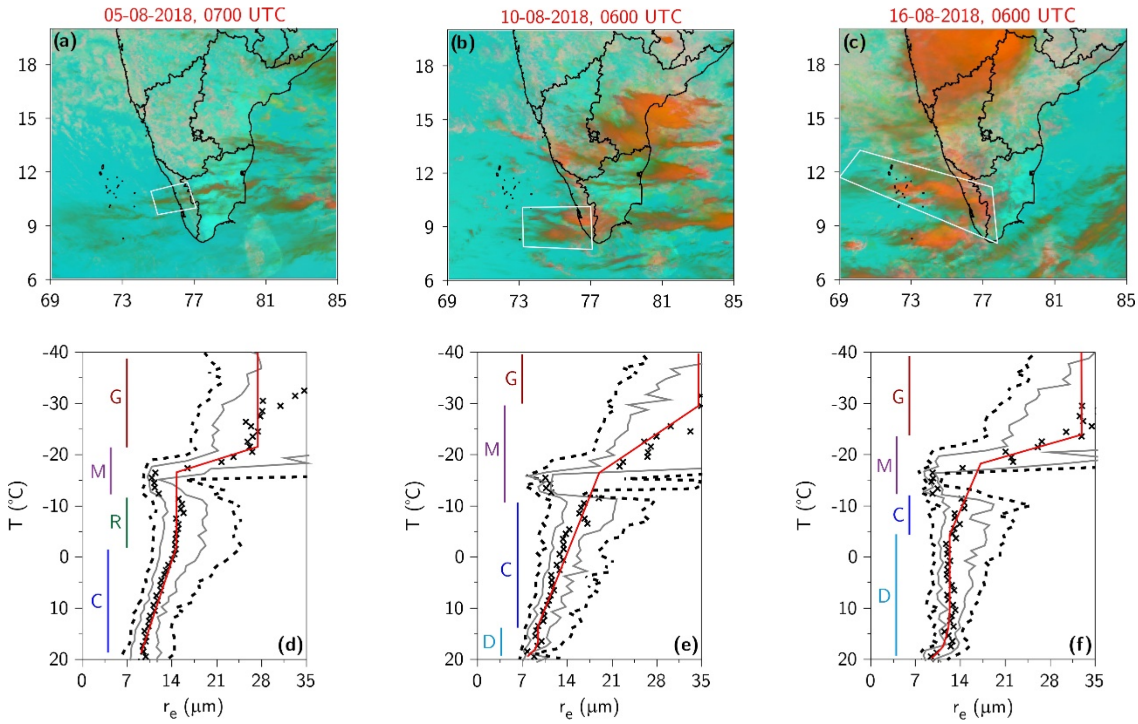

Fig. 5: Variation of the T-r$_e$ profiles between normal, heavy and extreme rainfall events: Cloud RGB composite image during **(a)** normal, **(b)** heavy, and **(c)** extreme rainfall events. The colour is composed of red for visible reflectance, green for 3.9 μm solar infrared temperature, and blue for 10.8 μm brightness temperature. The analysed cloud clusters are bounded in the white polygon. Vertical cloud microphysical structure of **(d)** normal, **(e)** heavy, and **(f)** extreme rainfall events. The 10, 25, 50, 75, and 90 percentiles of r_e are plotted. The vertical bars denote the vertical extent of the microphysical zones represented as D - diffusion, C - collision-coalescence, R - warm rainout, M - mixed phase, and G - glaciation.

Further evidence of a polluted scenario during ERE is ascertained from the delayed inception of the coalescence zone above the freezing level (Fig. 5f). Aircraft measurements reported similar cases of delayed coalescence zone up to the -5 °C isotherm in highly polluted environments over the Indo-Gangetic plains (Konwar et al., 2012). Supercooled raindrops at -12°C to -17°C are the primary initiators of precipitation in such clouds, indicating the presence of Ice Nuclei (IN) or giant CCN seeding the clouds. Insoluble aerosol particles, such as desert dust, are the primary natural sources of IN (Rosenfeld, 2018). The presence of giant CCN and dust particles (Supplementary Fig. 2) in a moist environment in the convective clouds developed over the geographical extent of the present study was pointed out by Konwar et al., 2014.

An interesting similarity was noted between the extreme and normal rainfall events in the glaciation zone, where the clouds in both the events are glaciated near -20°C. However, the underlined processes may be different in both cases. Although the heavy concentration of desert dust facilitates glaciation in clouds near -20°C (Ansmann et al., 2008), secondary ice formation processes, such as ice multiplication, can also glaciate clouds at this range (Rosenfeld and Woodley, 2000). Such ice multiplication processes become significant when cloud droplets grow larger than 12 μm (r_e) at a range of -3°C to -8°C (Hallett and Mossop, 1974). This is a characteristic of normal rainfall events, where the early collision-coalescence promotes the cloud drops to a larger radius (r_e > 12 μm). The glaciation in such cases occurs much warmer than those induced by the presence of desert dust (Rosenfeld et al., 2011). The occurrence of smaller cloud droplets (at the range of -3°C to -8°C) and glaciation colder than -20°C during EREs suggest the presence of dust aerosols and subsequent IN concentrations.

The updraft velocity does not affect the depth of diffusional zone for a given N_a, but it can delay the increase of r_e with height above the height of rain initiation (h (r_e~14 μm)) as there is less time for raindrop formation in the fast-rising parcel (Rosenfeld et al., 2007). Such strong updrafts are evident during EREs (Fig. 5f) from the steeper collision-coalescence zone. Moreover, the deeper diffusional zone of EREs dominated by condensation increases the column loading of condensed water and releases latent heat resulting in stronger updraft velocity. The r_e in such cases reaches the rain threshold (14 μm) at heights colder than 0 °C isotherms, making most of the cloud water available for mixed-phase processes. These processes release latent heat, further invigorating the updraft velocity (Li et al., 2011; Rosenfeld et al., 2008). Meenu et al. (2020) pointed out similar latent heat positive feedback during the analysis of the extreme event of 9 August 2018 using multi-satellite observations and numerical simulations. A sudden decrease in the r_e at the temperature range between -20°C and -18°C is observed consistently in all the rainfall events (Fig. 5). This could be due to the formation of ice crystals which commonly appear when the temperature is between -10°C and -15°C, though detailed analysis is required to reinforce this conclusion. The relatively low vapour pressure of ice causes water vapour to diffuse from many cloud droplets to fewer ice crystals (Lamb, 2003), thus reducing the cloud top r_e. Once the ice crystals attain sufficient sizes, cold cloud growth mechanisms are initiated, resulting in faster growth of r_e with further height.

3.3. Nowcasting of EREs

A logistic regression model was fitted for the rainfall of August 2018, and the estimated probabilities of normal and heavy/extreme rainfall events are shown in Fig. 6a. The plot shows a significantly higher probability during heavy and extreme rainfall events. At a probability cut-off of 0.5 for heavy and extreme rainfall events, the model shows an overall accuracy of 93%, illustrating the capability of the model for nowcasting the EREs. The efficiency of the model performance is evident from the receiver operating characteristic curve (Fig. 6b), which shows an area under the curve (AUC) of 0.97. Although we examined the capability of the model to nowcast different events between 2018 and 2021, hourly nowcasts of two selected heavy/extreme rainfall events of August 2018 over the region is demonstrated herein for brevity.

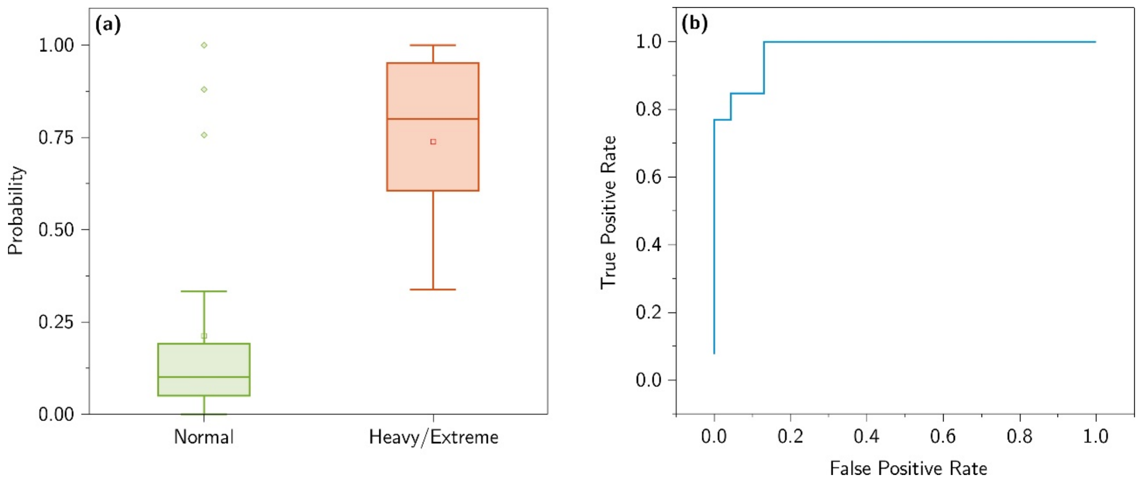

Fig. 6: Modelling of the occurrence of EREs: (a) Modelled probability for normal and heavy/extreme rainfall events during August 2018, and **(b)** the ROC curve for the logistic regression model. The effectiveness of the model was evaluated using the ROC curve with multiple events from 2018 to 2021.

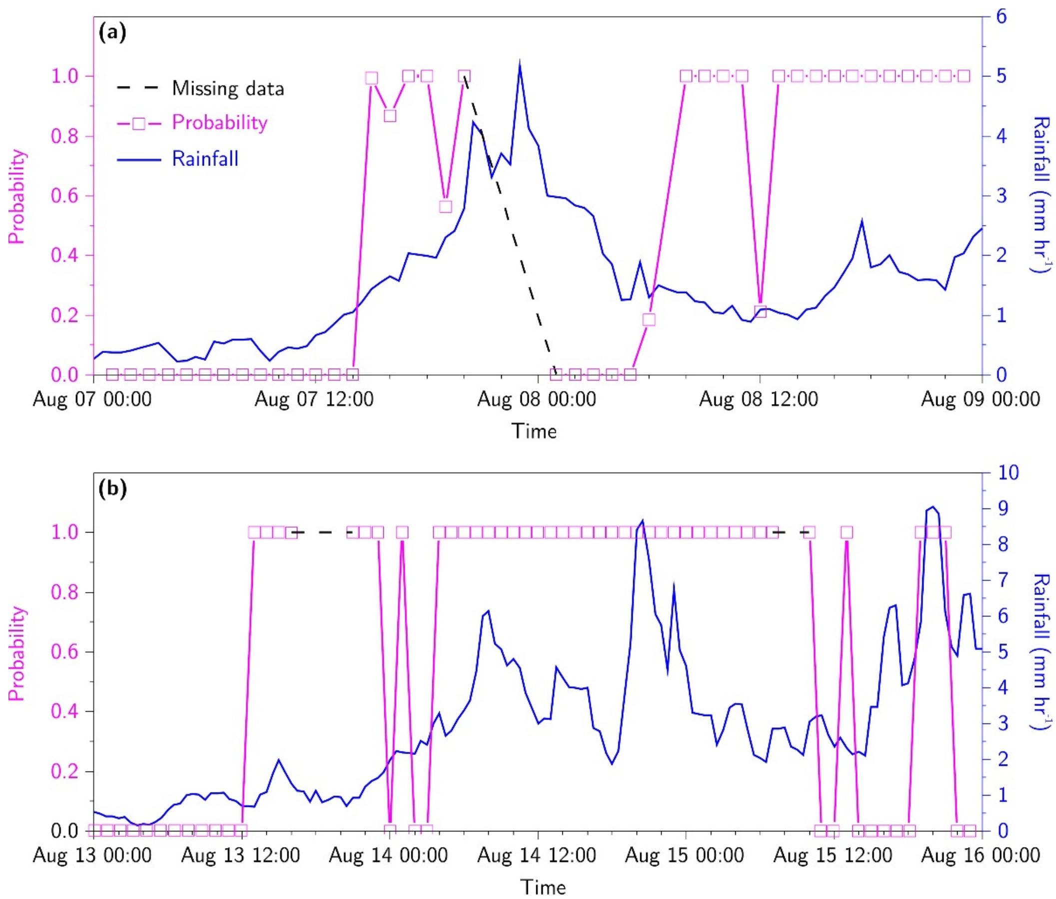

Fig. 7: Nowcasting of EREs: Nowcasting the heavy/extreme rainfall events of **(a)** 8 August 2018 and **(b)** 15 August 2018. The half-hourly gauge calibrated precipitation product from the IMERG was used to represent the temporal variation of rainfall.

On 8 August 2018, Kerala received heavy rainfall, followed by an ERE on 9 August. The rainfall rate of IMERG data suggests that the rainfall intensified around 9:00 PM on 7 August (Fig. 7a). The modelled probability for the occurrence of a heavy/ extreme rainfall event is also shown in Fig. 7a. The probability for a heavy/ extreme rainfall event remains low up to 2:00 PM on 7 August 2018, after which it shows a high probability for the occurrence. The modelled probability decreases during the early hours on 8 August, and a subsequent decrease in rainfall intensity are observed. However, from 8:00 AM onwards, the model shows high probability till 9 August, which is indicative of the ERE on 9 August 2018. Similarly, the rainfall rate of IMERG data indicates that Kerala received heavy rainfall on 14 August 2018, followed by EREs on 15, 16, and 17 August. The temporal pattern of the rainfall rate shows that rainfall intensified around 3:00 AM on 14 August (Fig. 7b). The modelled probability for a heavy/ extreme rainfall event remains low up to 12:00 PM on 13 August 2018, after which it shows a high probability for heavy/ extreme rainfall. The temporal variability of the modelled probability values of the first ERE (8-9 August 2018) shows the potential for the occurrence of a heavy/extreme rainfall event seven hours before the rainfall intensification. Similarly, during 15-17 August 2018, the technique provides a warning for the occurrence of a heavy/extreme rainfall event 15 hours before the rainfall intensification. The correlated variability between the rainfall intensity and the modelled probability generated by nowcasting indicates that the technique is capable of nowcasting the extreme rainfall event earlier to its intensification.

4. Summary and conclusion

This study proposed a technique to nowcast the heavy and extreme rainfall events using the early signatures of the microphysical evolution of mesoscale convective clouds. The nowcasting technique utilised different characteristics of the T-r_e profile, representing different microphysical stages of cloud development, and logistic regression modelling to estimate the probability for the occurrence of EREs. The capability of the method was demonstrated by nowcasting the different EREs that occurred in recent years across the southern Western Ghats (Kerala, India). It is noted that the interactions among the aerosol loading and moisture availability were also significant (other than their independent effects) in the occurrence of EREs of August 2018. The analysis of the T-r_e profiles of the normal, heavy and extreme rainfall events of August 2018 was significantly different and indicated a polluted (aerosol-rich) scenario. The deep diffusional zone and the delayed inception of the coalescence zone above the freezing level also indicated the significance of aerosols during EREs. The proposed technique showed distinctive competency for nowcasting the EREs at a regional scale with an overall accuracy of 93% and at a lead time of seven to fifteen hours. The results of this study emphasise the requirement for systematic and long-term monitoring and characterisation of aerosols to understand their role in the EREs of the region. The results help implement better policies to mitigate the impacts due to EREs and associated natural hazards.

Acknowledgements

This work was conducted under the DST project "Setting up of State Climate Change Knowledge Cell Under National Mission" at the Institute for Climate Change Studies, Kottayam. The authors acknowledge funding from the Department of Science and Technology (DST) (sanction number DST/SPLICE/CCP/NMSKCC/PR-62/2016 (G)), the Government of India.

Author contributions

KPS, JT, and PJJ conceptualised the study. SN conducted the data curation and data analysis. SN and JT interpreted and visualised the results and wrote the draft manuscript with specific inputs and edits from KPS and PJJ.

Competing interests

The authors declare that they have no known competing financial interests or personal relationships that could have appeared to influence the work reported in this paper.

References

Ahmed, F., Schumacher, C., 2015. Convective and stratiform components of the precipitation-moisture relationship. Geophys. Res. Lett. 42, 10453–10462. https://doi.org/10.1002/2015GL066957

Ansmann, A., Tesche, M., Althausen, D., Müller, D., Seifert, P., Freudenthaler, V., Heese, B., Wiegner, M., Pisani, G., Knippertz, P., Dubovik, O., 2008. Influence of Saharan dust on cloud glaciation in southern Morocco during the Saharan Mineral Dust Experiment. J. Geophys. Res. Atmos. 113, D04210. https://doi.org/10.1029/2007JD008785

Breugem, A.J., Wesseling, J.G., Oostindie, K., Ritsema, C.J., 2020. Meteorological aspects of heavy precipitation in relation to floods – An overview. Earth-Science Rev. 204, 103171. https://doi.org/10.1016/j.earscirev.2020.103171

Choudhry, P., Misra, A., Tripathi, S.N., 2012. Study of MODIS derived AOD at three different locations in the Indo Gangetic Plain: Kanpur, Gandhi College and Nainital. Ann. Geophys.

30, 1479–1493. https://doi.org/10.5194/angeo-30-1479-2012
Choudhury, G., Tyagi, B., Krishna Vissa, N., Singh, J., Sarangi, C., Nand Tripathi, S., Tesche, M., 2020. Aerosol-enhanced high precipitation events near the Himalayan foothills. Atmos. Chem. Phys. 20, 15389–15399. https://doi.org/10.5194/acp-20-15389-2020
Fortelli, A., Scafetta, N., Mazzarella, A., 2019. Nowcasting and real-time monitoring of heavy rainfall events inducing flash-floods: an application to Phlegraean area (Central-Southern Italy). Nat. Hazards 97, 861–889. https://doi.org/10.1007/s11069-019-03680-7
Fox, N. I. & Wikle, C. K. A Bayesian Quantitative Precipitation Nowcast Scheme. Weather Forecast. 20, 264–275 (2005).
Francis, P.A., Gadgil, S., 2006. Intense rainfall events over the west coast of India. Meteorol. Atmos. Phys. 94, 27–42. https://doi.org/10.1007/s00703-005-0167-2
Freud, E., Rosenfeld, D., 2012. Linear relation between convective cloud drop number concentration and depth for rain initiation. J. Geophys. Res. Atmos. 117. https://doi.org/10.1029/2011JD016457
Global Modeling and Assimilation Office (GMAO), 2015. Global Modeling and Assimilation Office (GMAO) (2015), MERRA-2 inst1_2d_asm_Nx: 2d,1-Hourly,Instantaneous,Single-Level,Assimilation,Single-Level Diagnostics V5.12.4, Greenbelt, MD, USA, Goddard Earth Sciences Data and Information Services Center (GES DISC).
Guo, L., Turner, A.G., Highwood, E.J., 2015. Impacts of 20th century aerosol emissions on the South Asian monsoon in the CMIP5 models. Atmos. Chem. Phys. 15, 6367–6378. https://doi.org/10.5194/acp-15-6367-2015f
Hallett, J., Mossop, S.C., 1974. Production of secondary ice particles during the riming process. Nature 249, 26–28. https://doi.org/10.1038/249026a0
Hamada, A., Takayabu, Y.N., Liu, C., Zipser, E.J., 2015. Weak linkage between the heaviest rainfall and tallest storms. Nat. Commun. 6, 6213. https://doi.org/10.1038/ncomms7213
He, S., Raghavan, S. V., Nguyen, N. S. & Liong, S.-Y. Ensemble rainfall forecasting with numerical weather prediction and radar-based nowcasting models. Hydrol. Process. 27, 1560–1571 (2013).
Huffman, G.J., Stocker, E.F., Bolvin, D.T., Nelkin, E.J., Tan, J., 2019. GPM IMERG Final Precipitation L3 Half Hourly 0.1 degree x 0.1 degree V06, Greenbelt, MD, Goddard Earth Sciences Data and Information Services Center (GES DISC).
Kaufman, Y.J., Tanré, D., Boucher, O., 2002. A satellite view of aerosols in the climate system. Nature 419, 215–223. https://doi.org/10.1038/nature01091
Khain, A., Rosenfeld, D., Pokrovsky, A., 2005. Aerosol impact on the dynamics and microphysics of deep convective clouds. Q. J. R. Meteorol. Soc. 131, 2639–2663. https://doi.org/10.1256/qj.04.62
Konwar, M., Das, S.K., Deshpande, S.M., Chakravarty, K., Goswami, B.N., 2014. Microphysics of clouds and rain over the Western Ghat. J. Geophys. Res. Atmos. 119, 6140–6159.

https://doi.org/10.1002/2014JD021606

Konwar, M., Maheskumar, R.S., Kulkarni, J.R., Freud, E., Goswami, B.N., Rosenfeld, D., 2012. Aerosol control on depth of warm rain in convective clouds. J. Geophys. Res. Atmos. 117. https://doi.org/10.1029/2012JD017585

Koren, I., Altaratz, O., Remer, L.A., Feingold, G., Martins, J.V., Heiblum, R.H., 2012. Aerosol-induced intensification of rain from the tropics to the mid-latitudes. Nat. Geosci. 5, 118–122. https://doi.org/10.1038/ngeo1364

Koren, I., Dagan, G., Altaratz, O., 2014. From aerosol-limited to invigoration of warm convective clouds. Science (80-.). 344, 1143–1146. https://doi.org/10.1126/science.1252595

Kumar, N., Kumar Goyal, M., Kumar Gupta, A., Jha, S., Das, J., Madramootoo, C.A., 2021. Joint behaviour of climate extremes across India: Past and future. J. Hydrol. 597, 126185. https://doi.org/10.1016/j.jhydrol.2021.126185

Kumar, S., Silva, Y., Moya-Álvarez, A.S., Martínez-Castro, D., 2019. Seasonal and regional differences in extreme rainfall events and their contribution to the world's precipitation: GPM observations. Adv. Meteorol. 2019. https://doi.org/10.1155/2019/4631609

Lamb, D., 2003. CLOUD MICROPHYSICS, in: Encyclopedia of Atmospheric Sciences. Elsevier, pp. 459–467. https://doi.org/10.1016/B0-12-227090-8/00111-1

Li, P. W. & Lai, E. S. T. Applications of radar-based nowcasting techniques for mesoscale weather forecasting in Hong Kong. Meteorol. Appl. 11, 253–264 (2004).

Li, Z., Niu, F., Fan, J., Liu, Y., Rosenfeld, D., Ding, Y., 2011. Long-term impacts of aerosols on the vertical development of clouds and precipitation. Nat. Geosci. 4, 888–894. https://doi.org/10.1038/ngeo1313

Lyngwa, R.V., Nayak, M.A., 2021. Atmospheric river linked to extreme rainfall events over Kerala in August 2018. Atmos. Res. 253, 105488. https://doi.org/10.1016/j.atmosres.2021.105488

Mao, J., Ping, F., Yin, L., Qiu, X., 2018. A Study of Cloud Microphysical Processes Associated With Torrential Rainfall Event Over Beijing. J. Geophys. Res. Atmos. 123, 8768–8791. https://doi.org/10.1029/2018JD028490

Meenu, S., Gayatri, K., Malap, N., Murugavel, P., Samanta, S., Prabha, T. V., 2020. The physics of extreme rainfall event: An investigation with multisatellite observations and numerical simulations. J. Atmos. Solar-Terrestrial Phys. 204, 105275. https://doi.org/10.1016/j.jastp.2020.105275

Metta, S., von Hardenberg, J., Ferraris, L., Rebora, N. & Provenzale, A. Precipitation nowcasting by a spectral-based nonlinear stochastic model. J. Hydrometeorol. 10, 1285–1297 (2009).

Minnis, P., Nguyen, L., Palikonda, R., Heck, P.W., Spangenberg, D.A., Doelling, D.R., Ayers, J.K., Smith, Jr., W.L., Khaiyer, M.M., Trepte, Q.Z., Avey, L.A., Chang, F.-L., Yost, C.R., Chee, T.L., Szedung, S.-M., 2008. Near-real time cloud retrievals from operational and research meteorological satellites, in: Picard, R.H., Comeron, A., Schäfer, K., Amodeo, A., van Weele, M. (Eds.), Remote Sensing of Clouds and the Atmosphere XIII. SPIE, p. 710703. https://doi.org/10.1117/12.800344

Misra, A., Jayaraman, A., Ganguly, D., 2015. Validation of Version 5.1 MODIS Aerosol Optical Depth (Deep Blue Algorithm and Dark Target Approach) over a Semi-Arid Location in Western India. Aerosol Air Qual. Res. 15, 252–262. https://doi.org/10.4209/aaqr.2014.01.0004

Mohandas, S., Francis, T., Singh, V., Jayakumar, A., George, J.P., Sandeep, A., Xavier, P., Rajagopal, E.N., 2020. NWP perspective of the extreme precipitation and flood event in Kerala (India) during August 2018. Dyn. Atmos. Ocean. 91, 101158. https://doi.org/10.1016/j.dynatmoce.2020.101158

Mukhopadhyay, P., Bechtold, P., Zhu, Y., Krishna, R.P.M., Kumar, S., Ganai, M., Tirkey, S., Goswami, T., Mahakur, M., Deshpande, M., Prasad, V.S., Johny, C.J., Mitra, A., Ashrit, R., Sarkar, A., Sarkar, S., Roy, K., Andrews, E., Kanase, R., Malviya, S., Abhilash, S., Domkawle, M., Pawar, S.D., Mamgain, A., Durai, V.R., Nanjundiah, R.S., Mitra, A.K., Rajagopal, E.N., Mohapatra, M., Rajeevan, M., 2021. Unravelling the mechanism of extreme (more than 30 sigma) precipitation during August 2018 and 2019 over Kerala, India. Weather Forecast. 36, 1253–1273. https://doi.org/10.1175/waf-d-20-0162.1

Nakajima, T., King, M.D., 1990. Determination of the Optical Thickness and Effective Particle Radius of Clouds from Reflected Solar Radiation Measurements. Part I: Theory. J. Atmos. Sci. 47, 1878–1893. https://doi.org/10.1175/1520-0469(1990)047<1878:DOTOTA>2.0.CO;2

Pai, D.S., Sridhar, L., Rajeevan, M., Sreejith, O.P., Satbhai, N.S., Mukhopadyay, B., 2014. Development of a new high spatial resolution (0 . 25× 0 . 25) Long Period (1901-2010) daily gridded rainfall data set over India and its comparison with existing data sets over the region. Mausam 65, 1–18.

Pattanaik, D.R., Rajeevan, M., 2010. Variability of extreme rainfall events over India during southwest monsoon season. Meteorol. Appl. 17, 88–104. https://doi.org/10.1002/met.164

Pulkkinen, S., Chandrasekar, V. & Harri, A. M. Stochastic spectral method for radar-based probabilistic precipitation nowcasting. J. Atmos. Ocean. Technol. 36, 971–985 (2019).

Putty, M.R.Y., Prithviraj, B.N., Kumar, P.N., Nithish, M.G., Giri, G., Chandramouli, P.N., 2021. An insight into the hydrological aspects of landslides of 2018 in Kodagu, South India. Landslides 18, 1597–1610. https://doi.org/10.1007/s10346-020-01589-y

Radhakrishna, B., Zawadzki, I. & Fabry, F. Predictability of Precipitation from Continental Radar Images. Part V: Growth and Decay. J. Atmos. Sci. 69, 3336–3349 (2012).

Rajeevan, M., Bhate, J., Jaswal, A.K., 2008. Analysis of variability and trends of extreme rainfall events over India using 104 years of gridded daily rainfall data. Geophys. Res. Lett. 35, L18707. https://doi.org/10.1029/2008GL035143

Ramanathan, V., 2001. Aerosols, Climate, and the Hydrological Cycle. Science (80-.). 294, 2119–2124. https://doi.org/10.1126/science.1064034

Ramanathan, V., Chung, C., Kim, D., Bettge, T., Buja, L., Kiehl, J.T., Washington, W.M., Fu, Q., Sikka, D.R., Wild, M., 2005. Atmospheric brown clouds: Impacts on South Asian climate and hydrological cycle. Proc. Natl. Acad. Sci. 102, 5326–5333. https://doi.org/10.1073/pnas.0500656102

Ravuri, S., Lenc, K., Willson, M., Kangin, D., Lam, R., Mirowski, P., Fitzsimons, M., Athanassiadou, M., Kashem, S., Madge, S., Prudden, R., Mandhane, A., Clark, A., Brock, A., Simonyan, K., Hadsell, R., Robinson, N., Clancy, E., Arribas, A., Mohamed, S., 2021. Skilful precipitation nowcasting using deep generative models of radar. Nat. 2021 5977878 597, 672–677. https://doi.org/10.1038/s41586-021-03854-z

Roca, R., Fiolleau, T., 2020. Extreme precipitation in the tropics is closely associated with long-lived convective systems. Commun. Earth Environ. 1, 18. https://doi.org/10.1038/s43247-020-00015-4

Rosenfeld, D., 2018. Cloud-Aerosol-Precipitation Interactions Based of Satellite Retrieved Vertical Profiles of Cloud Microstructure, in: Remote Sensing of Aerosols, Clouds, and Precipitation. Elsevier, pp. 129–152. https://doi.org/10.1016/B978-0-12-810437-8.00006-2

Rosenfeld, D., 2002. The Role of Sea Spray in Cleansing Air Pollution over Ocean via Cloud Processes. Science (80-.). 297, 1667–1670. https://doi.org/10.1126/science.1073869

Rosenfeld, D., 1999. TRMM observed first direct evidence of smoke from forest fires inhibiting rainfall. Geophys. Res. Lett. 26, 3105–3108. https://doi.org/10.1029/1999GL006066

Rosenfeld, D., Andreae, M.O., Asmi, A., Chin, M., De Leeuw, G., Donovan, D.P., Kahn, R., Kinne, S., Kivekäs, N., Kulmala, M., Lau, W., Schmidt, K.S., Suni, T., Wagner, T., Wild, M., Quaas, J., 2014. Global observations of aerosol-cloud-precipitation-climate interactions. Rev. Geophys. https://doi.org/10.1002/2013RG000441

Rosenfeld, D., Fromm, M., Trentmann, J., Luderer, G., Andreae, M.O., Servranckx, R., 2007. The Chisholm firestorm: Observed microstructure, precipitation and lightning activity of a pyro-cumulonimbus. Atmos. Chem. Phys. 7, 645–659. https://doi.org/10.5194/acp-7-645-2007

Rosenfeld, D., Lensky, I.M., 1998. Satellite–Based Insights into Precipitation Formation Processes in Continental and Maritime Convective Clouds. Bull. Am. Meteorol. Soc. 79, 2457–2476. https://doi.org/10.1175/1520-0477(1998)079<2457:SBIIPF>2.0.CO;2

Rosenfeld, D., Lohmann, U., Raga, G.B., O'Dowd, C.D., Kulmala, M., Fuzzi, S., Reissell, A., Andreae, M.O., 2008. Flood or drought: How do aerosols affect precipitation? Science (80-.). https://doi.org/10.1126/science.1160606

Rosenfeld, D., Woodley, W.L., 2000. Deep convective clouds with sustained supercooled liquid water down to -37.5 °C. Nature 405, 440–442. https://doi.org/10.1038/35013030

Rosenfeld, D., Yu, X., Liu, G., Xu, X., Zhu, Y., Yue, Z., Dai, J., Dong, Z., Dong, Y., Peng, Y.,

2011. Glaciation temperatures of convective clouds ingesting desert dust, air pollution and smoke from forest fires. Geophys. Res. Lett. 38, n/a-n/a. https://doi.org/10.1029/2011GL049423

Sarangi, C., Tripathi, S.N., Kanawade, V.P., Koren, I., Pai, D.S., 2017. Investigation of the aerosol–cloud–rainfall association over the Indian summer monsoon region. Atmos. Chem. Phys. 17, 5185–5204. https://doi.org/10.5194/acp-17-5185-2017

Sayer, A.M., Hsu, N.C., Bettenhausen, C., Jeong, M.-J., 2013. Validation and uncertainty estimates for MODIS Collection 6 “Deep Blue” aerosol data. J. Geophys. Res. Atmos. 118, 7864–7872. https://doi.org/10.1002/jgrd.50600

Schwartz, S.E., 1996. The whitehouse effect—Shortwave radiative forcing of climate by anthropogenic aerosols: an overview. J. Aerosol Sci. 27, 359–382. https://doi.org/10.1016/0021-8502(95)00533-1

Shukla, B.P., Kishtawal, C.M., Pal, P.K., 2017. Satellite-Based Nowcasting of Extreme Rainfall Events Over Western Himalayan Region. IEEE J. Sel. Top. Appl. Earth Obs. Remote Sens. 10, 1681–1686. https://doi.org/10.1109/JSTARS.2017.2655105

Sirangelo, B., Versace, P. & De Luca, D. L. Rainfall nowcasting by at site stochastic model P.R.A.I.S.E. Hydrol. Earth Syst. Sci. 11, 1341–1351 (2007).

Srinivas, C.V., Yesubabu, V., Hari Prasad, D., Hari Prasad, K.B.R.R., Greeshma, M.M., Baskaran, R., Venkatraman, B., 2018. Simulation of an extreme heavy rainfall event over Chennai, India using WRF: Sensitivity to grid resolution and boundary layer physics. Atmos. Res. 210, 66–82. https://doi.org/10.1016/j.atmosres.2018.04.014

Steinfeld, J.I., 1998. Atmospheric Chemistry and Physics: From Air Pollution to Climate Change. Environ. Sci. Policy Sustain. Dev. 40, 26–26. https://doi.org/10.1080/00139157.1999.10544295

Sun, J. et al. Use of nwp for nowcasting convective precipitation: Recent progress and challenges. Bull. Am. Meteorol. Soc. 95, 409–426 (2014).

Suzuki, K., Nakajima, T.Y., Stephens, G.L., 2010. Particle Growth and Drop Collection Efficiency of Warm Clouds as Inferred from Joint CloudSat and MODIS Observations. J. Atmos. Sci. 67, 3019–3032. https://doi.org/10.1175/2010JAS3463.1

Tawde, S.A., Singh, C., 2015. Investigation of orographic features influencing spatial distribution of rainfall over the Western Ghats of India using satellite data. Int. J. Climatol. 35, 2280–2293. https://doi.org/10.1002/joc.4146

Trenberth, K.E., Fasullo, J., Smith, L., 2005. Trends and variability in column-integrated atmospheric water vapor. Clim. Dyn. 24, 741–758. https://doi.org/10.1007/s00382-005-0017-4

Tripathi, S.N., Dey, S., Chandel, A., Srivastava, S., Singh, R.P., Holben, B.N., 2005. Comparison of MODIS and AERONET derived aerosol optical depth over the Ganga Basin, India. Ann. Geophys. 23, 1093–1101. https://doi.org/10.5194/angeo-23-1093-2005

Twomey, S., 1977. The Influence of Pollution on the Shortwave Albedo of Clouds. J. Atmos. Sci. 34, 1149–1152. https://doi.org/10.1175/1520-0469(1977)034<1149:TIOPOT>2.0.CO;2

Wang, R., Zhu, Y., Qiao, F., Liang, X.-Z., Zhang, H., Ding, Y., 2021. High-resolution Simulation of an Extreme Heavy Rainfall Event in Shanghai Using the Weather Research and Forecasting Model: Sensitivity to Planetary Boundary Layer Parameterization. Adv. Atmos. Sci. 38, 98–115. https://doi.org/10.1007/s00376-020-9255-y

Wilson, J. W., Crook, N. A., Mueller, C. K., Sun, J. & Dixon, M. Nowcasting Thunderstorms: A Status Report. Bull. Am. Meteorol. Soc. 79, 2079–2099 (1998).

Xavier, A., Kottayil, A., Mohanakumar, K., Xavier, P.K., 2018. The role of monsoon low-level jet in modulating heavy rainfall events. Int. J. Climatol. 38, e569–e576. https://doi.org/10.1002/joc.5390

Xiang, Y., Ma, J. & Wu, X. A Precipitation Nowcasting Mechanism for Real-World Data Based on Machine Learning. Math. Probl. Eng. 2020, 1–11 (2020).

Yunus, A.P., Fan, X., Subramanian, S.S., Jie, D., Xu, Q., 2021. Unraveling the drivers of intensified landslide regimes in Western Ghats, India. Sci. Total Environ. 770, 145357. https://doi.org/10.1016/j.scitotenv.2021.145357

Zhao, C., Wang, Y., Yang, Q., Fu, R., Cunnold, D., Choi, Y., 2010. Impact of East Asian summer monsoon on the air quality over China: View from space. J. Geophys. Res. 115, D09301. https://doi.org/10.1029/2009JD012745

Supplementary Material 1: Recent floods across Kerala

Kerala is the south-western State of India extending between 8° 18' - 12° 48' N latitude and 74° 52' - 77° 22' E longitude. The Arabian Sea borders the state in the west and the Western Ghats in the east. The state experiences mesoscale circulations during pre-monsoon and monsoon seasons, aggravated by local orographic disturbances due to the elevation gradient of the Western Ghats. The state receives an average annual precipitation of about 3,000 mm (CWC-Report, 2018), 70% of which is contributed by the Indian summer monsoon.

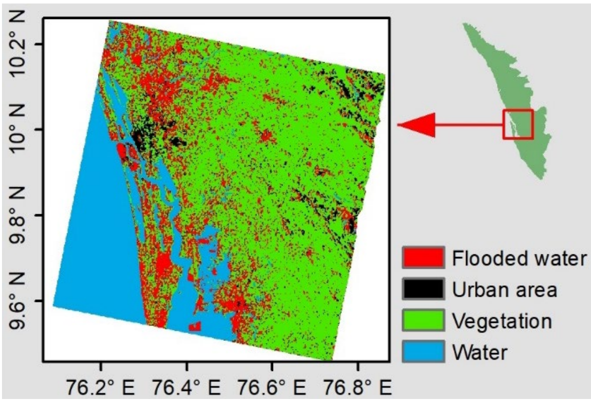

Fig S1: Flood-affected areas during the August 2018 floods over Kerala derived from the SENTINEL 1 SAR images.

The consecutive floods of large return periods over the state during 2018, 2019 and 2020 show an alarming situation of the rising EREs. Contrary to the long-term rainfall trends, Kerala experienced a remarkably higher amount of rainfall during the first half of the Indian summer monsoon season in 2018. During August 2018, the state experienced two severe EREs on record. During the first ERE (8 - 10 August 2018), a few meteorological stations of the state received more than 50% of the normal monthly rainfall in just three days. However, most of the state exceeded the normal monthly rainfall by 50% in the second ERE (15 - 17 August 2018), causing widespread flooding affecting almost 5.4 million people (KSCSTE-Report, 2019). Several districts were inundated for more than two weeks due to the floods. The analysis of SENTINEL-1 Synthetic Aperture Radar (SAR) data collected from NASA's Alaska Satellite Facility Distributed Active Archive Centre gives a visual perspective of the flood over central Kerala (Fig. S1). Comparison of pre- (16 July 2018) and post-flood (21 August 2018) SAR images reveal that roughly 22% (925 km^2) of the analysed area was inundated. About 341 major landslides were reported from ten districts during the EREs of August 2018, where 143 landslides ravaged the Idukki district.

The ERE occurred during August 2019 in Kerala was the result of the formation of a low-pressure system and later a depression over the northwest Bay of Bengal off north Odisha-West Bengal coasts on 6 August 2019. The widespread flooding and landslides across the districts of northern Kerala caused severe damage to both the built and natural ecosystems. The low-lying areas of the major river systems were inundated, and more than 2 lakh people were displaced. Kerala witnessed 80 landslides in eight districts over the three days (August 8-11, 2019) as the death toll crossed 120. However, the most devastating landslide witnessing the highest ever recorded casualty occurred during the EREs in 2020 in Pettimudy, Idukki. While most of the landslides in the state during recent years were primarily triggered by the EREs, anthropogenic interferences also contributed to the instability of the slopes (KSCSTE-Report, 2019). However, most recent landslide events show no significant changes in land use, suggesting the significant role of the extraordinary rainfall events (Martha et al., 2019)

Supplementary Material 2: Wind Trajectory computations

The wind trajectory vectors were analysed to understand the wind patterns and aerosol transport pathways over Kerala using the PC-Windows-based NOAA HYSPLIT model (Rolph et al., 2017; Stein et al., 2015). Seven days backward trajectories were computed every hour at 850 hPa from a central location (10.5°N, 76.3°E) over Kerala. These trajectories were then clustered to an optimal number of clusters based on the total spatial variance explained by the clusters (Fig. S2). The analysis was performed for 2001 and 2018 using the 2.5° NCEP reanalysis data.

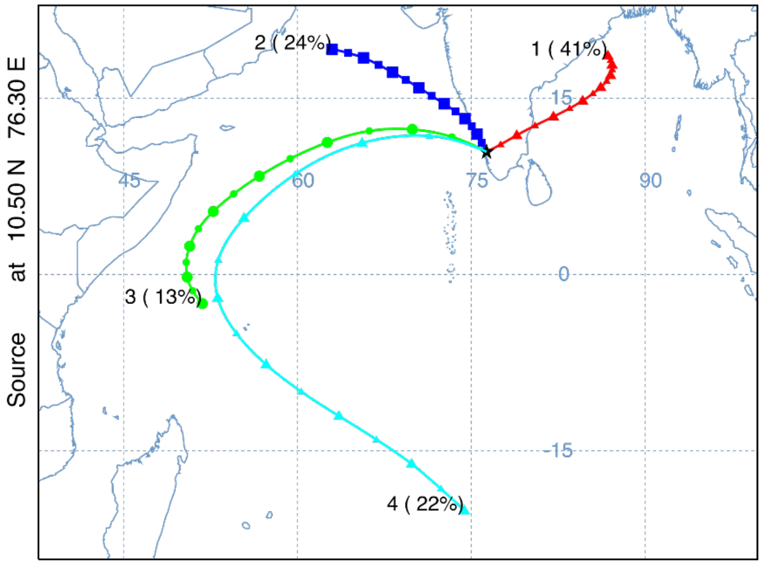

Fig S2: Wind trajectory clusters from a central location (10.5°N, 76.3°E) over Kerala during 2001

Supplementary Material 3: Aerosol variation over Kerala

The atmospheric aerosols with hygroscopic properties act as CCN over which water condenses, and hence their variation can impact cloud formation and further precipitation. The time-series of the AOD over Kerala as observed from the MODIS is shown in Fig. S3. The Mann-Kendall trend test indicates a significantly increasing AOD over the region since the beginning of the 21st century, implying the increasing concentration of aerosols. Various researchers reported such observations in Thiruvananthapuram (Kerala) using ground-based measurements (Moorthy and Satheesh, 2000). They observed a peak AOD during the monsoon season and reported its primary contribution from sea-salt aerosols with occasional contributions from transported desert dust. They also noted an increasing trend in AOD due to an increase in urbanisation and other anthropogenic sources.

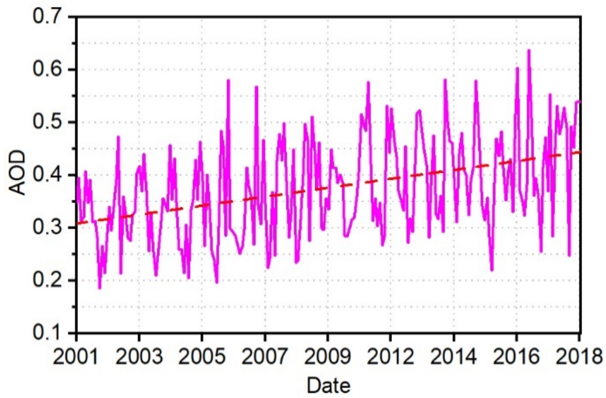

Fig S3: Temporal variation of AOD over Kerala from 2001 to 2018.

References

Martha, T.R., Roy, P., Khanna, K., Mrinalni, K., Vinod Kumar, K., 2019. Landslides Mapped using Satellite Data in the Western Ghats of India After Excess Rainfall During August 2018. Curr. Sci. 117, 804. https://doi.org/10.18520/cs/v117/i5/804-812

Moorthy, K.K., Satheesh, S.K., 2000. Characteristics of aerosols over a remote island, Minicoy in the Arabian Sea: Optical properties and retrieved size characteristics. Q. J. R. Meteorol. Soc. 126, 81–109. https://doi.org/10.1002/qj.49712656205

Rolph, G., Stein, A., Stunder, B., 2017. Real-time Environmental Applications and Display sYstem: READY. Environ. Model. Softw. 95, 210–228. https://doi.org/10.1016/j.envsoft.2017.06.025

Stein, A.F., Draxler, R.R., Rolph, G.D., Stunder, B.J.B., Cohen, M.D., Ngan, F., 2015. NOAA's HYSPLIT Atmospheric Transport and Dispersion Modeling System. Bull. Am. Meteorol. Soc. 96, 2059–2077. https://doi.org/10.1175/BAMS-D-14-00110.1